Journal of Solid State Chemistry 182 (2009) 1708–1712

Contents lists available at ScienceDirect

Journal of Solid State Chemistry

journal homepage: www.elsevier.com/locate/jssc

Structural and compositional investigations of Zr_4Pt_2O: A filled-cubic Ti_2Ni-type phase

Shalabh Gupta [a], Daniel J. Sordelet [b], John D. Corbett [a,*]

[a] Ames Laboratory-DOE and Department of Chemistry, Iowa State University, Ames, IA, USA 50011
[b] Materials and Engineering Physics Program, Ames Laboratory, Iowa State University, Ames, IA, USA 50011

ARTICLE INFO

Article history:
Received 16 January 2009
Received in revised form
2 April 2009
Accepted 5 April 2009
Available online 18 April 2009

Keywords:
Crystal structure
Stuffed Ti_2Ni structure
$Zr_5Pt_3O_x$
Zr–Pt–O system
Stoichiometry

ABSTRACT

Syntheses, structural and compositional analyses of the filled cubic Ti_2Ni-type phase in Zr–Pt–O system have been studied, largely for the platinum-richer compositions. Diffraction quality crystals were grown by annealing an arc-melted composition $Zr_4Pt_2O_{0.66}$ at 1600 °C under Ar. The refined composition $Zr_{4.0}Pt_{1.95(1)}O_{0.93(6)}$ ($a = 12.5063(6)$ Å, $Fd\bar{3}m$, $Z = 16$) is close to the idealized composition Zr_4Pt_2O known in several other Zr–T–O systems (T = late 4*d* or 5*d* transition element). (This composition has been erroneously reported by ICDD for years as Zr_6Pt_3O (No. 00-017-0557) and referred to as ε-Zr_6Pt_3O.) The product is only marginally poor in platinum and oxygen, in contrast to the 1960 reports of metallographic studies ($\sim Zr_4Pt_{1.62}O_{0.44}$). Under arc-melting conditions, high yields of the cubic phase are obtained from samples with lower platinum concentrations ($Zr_4Pt_{1.74}O_{1.04}$), whereas samples near the refined cubic composition contain hexagonal $Zr_5Pt_3O_x$ as well (Mn_5Si_3-type). The hexagonal structure of binary Zr_5Pt_3 was also refined (Mn_5Si_3 type, $P6_3/mcm$, $a = 8.210(1)$ Å, $c = 5.385(2)$ Å) and shown to be non-stoichiometric to at least $Zr_5Pt_{2.5}$.

1. Introduction

Interest in filled cubic Ti_2Ni-type intermetallic compounds has grown in recent years because of its preferential nucleation during glass forming reactions in various metallic alloy systems. Cubic Ti_2Ni-type structures ($Fd\bar{3}m$) [1,2] have been characterized for a large number of early and late transition metal combinations. The first (1939) report on Ti_2Ni described the structure (correctly) as face-centered cubic with 96 atoms in the unit cell. The complete structure was described by Yurko et al. [3] who on the basis of intensities from powder diffraction and systematic absence conditions assigned $Fd\bar{3}m$ as the most probable space group. The 48*f* and 16*d* sites for Ti and the 32*e* site for Ni were proposed on the basis of distance considerations. The first single crystal investigation on the isotypic filled Ti_2Ni-type for Zr_4Ni_2O by Franzen et al. [4] confirmed the earlier structural details and also established the interstitial oxygen on the 16*c* site. In its most general form, filled Ti_2Ni-type structure can be described as $M^1_3M^2T_2O$ in which M^1 and M^2 may be the same or different early transition metals and T is a late transition metal.

Several metal combinations such as Zr with Rh, Ir or Pt and Hf with Rh, Pd, Ir or Pt give the cubic phase only with more or less major amounts of interstitial oxygen, which yield the filled cubic-Ti_2Ni structures with strong M–O bonding particularly with the early transition metal [5,6]. A net gain in energy is reportedly achieved from metal–oxygen bonding at the expense of the metal–metal bonds [4]. The lower and the upper limits of oxygen in these ternary systems have been understood in a qualitative sense in terms of chemical valence of later transition metal component and the maximum filling of the 16*c* oxygen sites, respectively [7]. For example, in the Ti_2X series, X = Cr, Mn, Fe, Co, Ni, or Cu, both binary and ternary Ti_2Ni type phases exist in the Ni and Cu systems, whereas the valence-electron-poorer Ti_2Fe analog exists only with oxygen. Following the higher normal oxidation states of Cr and Mn compared with Fe, the minimum oxygen limits for the filled-phase in Ti_2MnO_x and Ti_2CrO_y systems are also higher [7,8]. The cubic phases in the Zr–Co and Zr–Ni systems are stable only with oxygen. Apart from the variable oxygen stoichiometries in the ternary compounds, variation in the metal ratios from 2:1 (48*f* and 16*d* sites occupied by same metal) as in Zr_4Ni_2O) to 1:1 (48*f* (Nb) and 32*e*+16*d* (Ni) in Nb_6Ni_6O) have also been observed. Oxygen ordering at either 16*c* or the 8*a* sites correlates with the early transition metal atom positions. For example, oxygen preferentially orders at the 8*a* site in Nb_6Ni_6O whereas it exclusively occupies the 16*d* sites in Zr_4Ni_2O [4].

Oxygen in Zr–Pt–O alloys recently investigated by Sordelet et al. was found to play a decisive role in limiting the formation of a binary Zr–Pt glassy alloy [9]. An increased proportion of the crystalline filled-cubic oxide appeared with increasing oxygen concentrations rather than a β-Zr(Pt) superstructure or the

* Corresponding author.
E-mail address: jdc@ameslab.gov (J.D. Corbett).

0022-4596/$ - see front matter © 2009 Elsevier Inc. All rights reserved.
doi:10.1016/j.jssc.2009.04.011

icosahedral quasicrystalline phase. Electron microscopic investigations revealed a close orientational relationship between these three phases in rapidly solidified eutectic alloys of nominal $Zr_{80}Pt_{20}$. Hence, a clearer elucidation of the composition and width of the filled-cubic phase $Zr_4Pt_2O_x$ should allow a better understanding of the formation of the competing phases. Furthermore, the Zr:*X* metal proportions in the oxide, especially for *X* from the 4*d* and 5*d* series, appeared to be greater than 2.0 according to an earlier report [7], but this remains in contrast to the Zr_4Ni_2O analog for which no Zr:Ni non-stoichiometry was found [4]. Given the current interest in alloys in the Zr–Pt–O system, a better determination of the composition range of the filled-cubic phase seemed necessary. Furthermore, the composition of this filled-cubic phase, cited in a database for many years as ε-Zr_6Pt_3O (ICDD No. 00-017-0557 [10]), is at variance with the earlier reports and calls for reassessment.

2. Experimental section

2.1. Syntheses

All samples were prepared by arc-melting pelletized mixtures of high purity Zr (0.25 mm foil, Alfa-Aesar, 99.9%, O<50 ppm mass), Pt (0.25 mm foil, Ames Laboratory, 99.95%) and ZrO_2 powder (Johnson Matthey, 99.9%). For a typical reaction, approximately 500 mg of an appropriate mixture of Zr, Pt and ZrO_2 was pelletized and arc-melted on a water-cooled Cu hearth under flowing argon inside a glove box. The pellets were then flipped and re-melted to promote homogenization. These samples needed no further annealing except in the case in which larger crystals were grown. Weight loss during arc-melting in all cases was insignificant (<0.1%). A comprehensive list of ten ternary reactions, their products and yields is given in Table 1. Also, the arc-melted pellets from binary Zr–Pt reactions (Table 1) and one ternary composition Zr_5Pt_3O, were further reacted at 1300 °C for 12 h in a vacuum furnace (Thermal Technology Inc. Model 1000A, $<10^{-6}$ Torr) followed by radiative cooling. Crystals of the cubic phase together with Zr_5Pt_3 were obtained by reaction of the arc-melted pellet of $Zr_4Pt_2O_{0.66}$ (wrapped in Ta foil and further sealed within Ta container under argon) at 1600 °C for one week under flowing Ar in a high temperature furnace (M60, Centorr/Vacuum Industries, Nashua, NH). The starting composition Zr_6Pt_3O ($Zr_4Pt_2O_{0.66}$) was chosen on the basis of the earlier but incorrect description of the composition of the cubic oxide in this system [10].

All products were analyzed with the aid of powder diffraction patterns secured with a Huber 670 Guinier (image-plate) and Cu$K\alpha_1$ radiation ($\lambda = 1.540598$ Å, $4^\circ \leqslant 2\theta \leqslant 100^\circ$, step width 0.005°) at ambient temperature. Yield distributions on a volume percent basis for the two major phases, cubic Ti_2Ni-type and hexagonal Mn_5Si_3-type, were estimated by comparison of the product powder patterns relative to those calculated according to the respective single crystal refinement data. A conservative estimate of the detection limit of foreign phases is 5%. Lattice constants for both phases were refined from the powder pattern data using WinXPow [11]. Both cubic and the hexagonal phase appear to be stable in air at room temperature for months.

Heavy element compositions of the two phases were determined with the aid of a scanning electron microscope (SEM: JEOL JSM 6100, Peabody, MA) equipped with an energy dispersive spectrometer (EDS, Oxford Instruments, Valley, CA). The metal ratios by EDS agreed reasonably well with the expected heavy atom compositions: $Zr_{4.1(2)}Pt_{2.0(1)}$ for the cubic and $Zr_{4.9(2)}Pt_{3.0(2)}$ for the hexagonal phases. Oxygen analyses were done by inert gas fusion of the sample with the starting composition $Zr_4Pt_2O_{0.66}$ before and after annealing. The first result was in good agreement with the initial composition (1.30(8) wt% O), and no significant oxygen uptake during annealing was observed. Likewise, the change in the cubic lattice constant was negligible.

2.2. Structure determinations

Irregular metal-looking crystals were separated from the crushed sample, mounted on a glass fiber, and checked for

Table 1
Reaction products, yields (vol%), and refined lattice constants for filled-cubic and hexagonal Zr–Pt–O phases refined from Guinier powder pattern data.

	Loaded comp., cond.[a]	Products[b] and yield	Lattice const.[c] (Å)	*V* (Å^3)
1.	$Zr_4Pt_2O_{0.13}$	H major phase (broad peaks), A broad hump		
2.	$Zr_4Pt_2O_{0.33}$	H~95% (broad peaks)	*a = 8.171(2), c = 5.3719(6)*	*311.10(9)*
3.	$Zr_4Pt_2O_{0.66}$	C (65%)+H (35%)	12.506(1)	1955.9(3)
			a = 8.172(1), c = 5.3719(6)	*310.71(5)*
4.	Sample 3 (1600 °C, 5 days)	C (80%)+H (20%)	12.5063(6)	1956.1(2)
5	$Zr_4Pt_2O_{1.0}$	C (60%)+H (40%)	12.5028(9)	1954.4(2)
			a = 8.1630(1), c = 5.3505(1)	*308.68(1)*
6.	$Zr_4Pt_2O_{1.2}$	C (42%)+H (~53%) + ZrO_2 (5%)	12.502(1)	1954.3(4)
			a = 8.169(2), c = 5.372(1)	*310.5(1)*
7.	$Zr_4Pt_2O_{1.5}$	H>90%+ZrO_2 (5%)	*a = 8.169(1), c = 5.373(1)*	*310.58(9)*
8.	$Zr_4Pt_{1.78}O_{1.07}$	C (90%)+H (10%)	12.4954(7)	1951.0(2)
9.	$Zr_4Pt_{1.74}O_{1.04}$	C (~95%)	12.496(4)	1951.2(1)
10.	$Zr_4Pt_{2.5}O_{1.2}$	H~85%, unknown 15%	*a = 8.169(4), c = 5.368(2)*	*310.3(1)*
Zr_5Pt_3				
11.	$Zr_5Pt_{2.5}$	H~95%	*a = 8.1897(9), c = 5.375(1)*	*312.18(7)*
12.	$Zr_5Pt_{2.75}$	H~95%	*a = 8.197(2), c = 5.379(2)*	*313.0(1)*
13.	Zr_5Pt_3	*H~95%*	*a = 8.207(1), c = 5.384(2)*	*314.1(1)*
14.	$Zr_5Pt_{3.25}$	H~90%+unidentified phase	*a = 8.203(1), c = 5.3811(7)*	*313.61(5)*
15.	Zr_5Pt_3O	H~90%	*a = 8.1662(8), c = 5.3708(6)*	*310.18(4)*
16.	$Zr_5Pt_{1.9}O_{2.4}$ (= $Zr_4Pt_{1.5}O_{1.9}$)	C (50%)+H (50%)+ZrO_2	12.507(2)	1956.4(5)
			a = 8.169(1), c = 5.3722(8)	*310.47(6)*

[a] All samples were first arc-melted. The Zr–Pt samples and Zr_5Pt_3O (15) were further reacted at 1300 °C for 12 h.
[b] C: cubic filled-Ti_2Ni type $Zr_4Pt_2O_x$; H: hexagonal Mn_5Si_3-type Zr_5Pt_3O.
[c] Cell dimensions of hexagonal phases are italicized.

singularity. Intensity data were collected from the best with the aid of a Bruker APEX CCD-based X-ray diffractometer over a sphere of reciprocal space to $2\theta_{max} = 56.58^\circ$ with 10 s/frame exposures. The reflection intensities were integrated with SAINT-PLUS 6.22 [12] program using a narrow-frame algorithm, and absorption effects were corrected empirically by means of the SADABS routine [13] to give 5373 total reflections, out of which 146 were independent ($R_{int} = 0.037$) and observed ($I > 2\sigma_I$). Space group $Fd\bar{3}m$ was selected on the basis of systematic absence conditions and prior knowledge. The structure was solved by direct methods and refined on F^2 with the aid of SHELXTL 6.10 [14]. Details of data collection and crystal data are listed in Table 2. The initial solution located three metal atoms that were assigned as Zr (48*f* and 16*d*) and Pt (32*e*) according to the single crystal report on Zr_4Ni_2O [4]. The refinement converged quickly; however, a residual electron density 2.33 Å from the 48*f* Zr positions could be clearly seen, and this was eventually refined as oxygen. At this time U_{iso} values for 16*d* and 32*e* sites assigned as Zr2 and Pt, respectively, were about four times those for Zr1 at 48*f* site. The possibility of fractional occupancies at these metal sites was checked in a separate least-squares cycles, but none showed any significant fractional occupancy. An oxygen site occupancy refinement gave ~97(1)% occupancy, which was retained at full occupancy. The model was then refined anisotropically, for which higher *Ueq* values persisted for Zr2 (23(1)) and Pt (18(1)) relative to Zr1 (6(1)). This was attributed to the different bonding environments of these atoms, as discussed later. Refinement of Pt occupancy in the anisotropic model afforded a slight improvement in overall refinement with a marginal 0.971(7). Anisotropic refinement of oxygen site occupancy also gave a marginal partial occupancy (0.93(6)) with significant decrease in its *Ueq* (8(4)). The final least-squares refinements, with anisotropic displacement parameters, and fractional Pt and O sites, converged at $R1 = 1.93\%$, $wR2 = 4.85\%$, and GoF = 1.133, with 16 parameters refined from 146 independent reflections. The final refined composition was thus $Zr_{4.0}Pt_{1.94(1)}O_{0.93(6)}$.

Some crystal and refinement details are presented in Table 2, and atomic coordinates along with the isotropic-equivalent displacement parameters are in Table 3. Anisotropic displacement parameters are listed in Table 4. The atomic coordinates have been standardized with the STRUCTURE TIDY program [15], and the interatomic distances in Table 5 were calculated using unit cell parameters obtained from Guinier data.

Table 2
Crystal data and structure refinement parameters for $Zr_{4.0}Pt_{1.95(1)}O_{0.93(6)}$.

fw	771.06
Temperature (K)	293(2)
Wavelength (Å)	0.71073
Crystal system	Cubic
Space group (*Z*)	$Fd\bar{3}m$; 16[b]
a[a] (Å)	12.5063(6)
V (Å^3)	1956.01(1)
d_{calcd} (g/cm^3)	10.46
μ, (mm^{-1}) (Mo*K*α)	64.956
Reflections collected	5373
Indep. Ref., [*R*(int)]	146 [*R*(int) = 0.0373]
Data/para.	146/16
GoF on F^2	1.133
*R*1, *wR*2 [$I > 2\sigma(I)$][c]	0.0193, 0.0485
*R*1, *wR*2 (all data)[c]	0.0196, 0.0490

[a] Obtained from Guinier powder diffraction data.
[b] Origin at $\bar{4}3m$.
[c] $R1 = \sum(Fo - Fc)/\sum|Fo|$; $wR2 = \{\sum w[(Fo^2 - Fc^2)^2]/\sum w[(Fo^2)^2]\}^{1/2}$.

Table 3
Atomic coordinates and isotropic-equivalent displacement parameters (Å$^2 \times 10^3$) for $Zr_{4.0}Pt_{1.95(1)}O_{0.93(6)}$.

	Wyck.	occ.≠1	*x*	*y*	*z*	*U*(*eq*)
Zr1	48*f*		0.1852(1)	0	0	6(1)
Pt	32*e*	0.971(7)	0.8443(1)	0.8443(1)	0.8443(1)	18(1)
Zr2	16*d*		5/8	5/8	5/8	23(1)
O	16*c*	0.93(6)	1/8	1/8	1/8	8(4)

Table 4
Anisotropic displacement parameters (Å$^2 \times 10^3$) for $Zr_{4.0}Pt_{1.95(1)}O_{0.93(6)}$.

	$U^{11} = U^{22} = U^{33}$	$U^{23} = U^{13}$	U^{12}
Zr1	7(1)	0	−1(1)
Pt	18(1)	0(1)	0(1)
Zr2	23(1)	16(1)	16(1)
O	8(5)	−1(3)	−1(3)

Table 5
Interatomic distances (Å) in $Zr_{4.0}Pt_{1.95(1)}O_{0.93(6)}$[a].

O	Zr1	×6	2.3355(4)
	Pt	×6	3.5520(1)
Zr1	O	×2	2.3355(4)
	Pt	×2	2.7781(5)
	Pt	×2	3.2228(9)
	Zr2	×2	3.2438(8)
	Zr1	×4	3.275(1)
	Zr1	×4	3.331(1)
Pt	Zr1	×3	2.7781(5)
	Zr2	×3	2.7960(3)
	Zr1	×3	3.2228(9)
	Pt	×3	3.336(1)
Zr2	Pt	×6	2.7960(3)
	Zr1	×6	3.2438(8)

[a] Calculated from Guinier lattice constants.

2.3. Electronic structure calculations

The electronic structure of the refined cubic phase (with full occupancies) was calculated self-consistently by the tight-binding linear muffin-tin-orbital (TB-LMTO) method [16–19] within the atomic sphere approximation (ASA) using the Stuttgart code [20]. Exchange and correlation were treated in a local spin density approximation (LSDA) [21], and scalar relativistic effects [22] were taken into account. The radii of Wigner–Seitz (WS) spheres were optimized by requiring that the overlapping potentials be the best possible approximations to the full potential according to an automatic procedure [23]. The WS radii so determined are in the ranges 2.97–3.12 Å for Zr, 2.88 Å for Pt, and 1.12–1.56 Å for the six empty spheres necessary to complete the potential. The basis set included 5*s*, 5*p*, and 4*d* functions for Zr, 6*s*, 6*p*, and 5*d* functions for Pt, 2*s* and 2*p* functions for O, and a 1*s* function for the empty spheres. Reciprocal space integrations to determine self-consistent charge densities, density of states (DOS) curves, and crystal orbital Hamilton population (COHP) [24] analyses were performed by the tetrahedron method [25] with 145 *k*-points in the irreducible wedges of the corresponding Brillouin zone.

3. Results and discussion

3.1. Syntheses

3.1.1. The ternary oxides

Several synthesis reactions were carried out with $Zr_4Pt_2O_x$ ($0.13 \leqslant x \leqslant 1.5$) compositions, Table 1. Arc-melting those with 2–5 at% oxygen (samples 1 and 2) yielded only hexagonal Zr_5Pt_3 type phases in >90% yields. The cubic phase mixed with the hexagonal member was observed with oxygen concentrations of ~10 at% or higher (3,5,6). However, not more than 70% of the cubic oxide phase could be obtained in any case because of the competitive hexagonal phase around this point. The Zr_4Pt_2 ($Zr_5Pt_{2.5}$) composition in the mixture is Pt-poor relative to the hexagonal Zr_5Pt_3 (Mn_5Si_3-type) structure, and the best yields of the cubic phase, 90–95%, were thus obtained from $Zr_4Pt_{\sim 1.75}O_{\sim 1.0}$ compositions (8,9). The cubic cell volume is around 1954–1956 Å^3 in equilibrium with the hexagonal phase (3,6,7) but decreases to ~1951 Å^3 with no hexagonal phase present and less Pt, all for arc-melted products (above). Oxygen analyses on mixed phase $Zr_4Pt_2O_{0.66}$ samples before and after annealing (to gain larger crystals) did not indicate any significant oxygen uptake during this process. This is also reflected in the unchanged lattice parameters obtained for these cubic phases.

Lattice volumes of the hexagonal phase in the ternary system are significantly reduced ($\Delta V \sim 3$ Å^3) as compared with that of Zr_5Pt_3 (below) obtained from stoichiometric reactions, however (13,15), suggesting oxygen uptake by the hexagonal lattice in the former. This is a general characteristic of many, and maybe most, compounds with a Mn_5Si_3-type structure [26]. It is relevant here to mention the similar case of Zr_4Ni_2O in which a pure cubic phase could not be obtained from typical high temperature solid state reactions even for stochiometric compositions [4].

3.1.2. The binary Zr–Pt system

A recently published phase diagram [27] for the binary Zr–Pt system shows no homogeneity range for the hexagonal $Zr_5Pt_{3\pm}$ phase, in contrast to an earlier report [28]. However, in the present work, lattice constants of hexagonal products gained in at least 80% yield from binary reactions of variable compositions suggested a substantial phase width (Table 1). In order to characterize the cubic phase width better, a more detailed characterization of the hexagonal phase became imperative, and this included the first single crystal investigation of the single phase product obtained from a stoichiometric Zr_5Pt_3 reaction. Details of data collection and refinement parameters are included in the Supplementary material.

Reactions in binary Zr–Pt system with sub-stoichiometric amounts of platinum at 1300 °C (samples 11 and 12) gave high yields (>95%) of the hexagonal phase with marginally smaller cell volumes ($\Delta V = 1.9(1)$ Å^3) from Zr_5Pt_3 down to $Zr_5Pt_{2.5}$. A $Zr_5Pt_{3.25}$ reaction under same conditions (sample 14) gave the hexagonal product in equilibrium with unknown phase but with a cell volume close to that of the stoichiometric composition. Smaller cell volumes for high yield reactions with decreasing Pt provide evidence for a modest phase width in the binary Zr_5Pt_{3-x} ($0 \leqslant x \leqslant 0.5$). The synthetic results clearly indicate that the hexagonal phase limits the stoichiometry of the cubic phase on both the high Pt and high oxygen sides, and this makes a precise determination of the cubic phase width difficult.

3.2. Structures

The structure of $Zr_{4.0}Pt_{1.95(1)}O_{0.93(6)}$, Fig. 1, can be described as an three-dimensional network of two interpenetrating and interlinked substructures; namely, a network of Zr1 (48*f*) octahedra (central, heavy outline) connected in such a way that these empty octahedra share four alternate faces with other Zr1 octahedra that are centered by O (16*c*) which in turn share two trans faces with empty octahedra. The leftover vacant space is filled with a second substructure, corner-connected stella quadrangulae built of central empty tetrahedra of Pt (32*e*) capped on all four faces by Zr2 (16*d*).

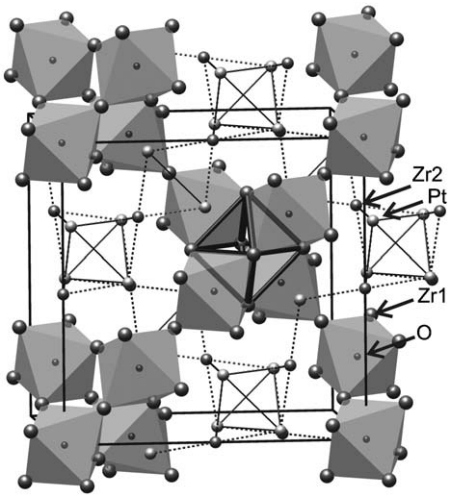

Fig. 1.

The higher *Ueq* refined for Zr2 and Pt can be explained on the basis of the coordination polyhedra around these sites. The major Zr1 atoms are strongly bonded to two oxygen atom (2.3355 (4) Å) within its 16-atom shell (10Zr+4Pt+2O) whereas Zr2 (6Zr+6Pt) and Pt (9Zr+3Pt) have only 12 bonded neighbors with no oxygen. The average Zr–Zr and Pt–Pt distances are 3.270(1) and 3.336(1) Å, respectively, which are much longer than their single bond radius sum (2.91 and 2.39 Å respectively [29]). One the other hand, the average heteroatomic Zr–Pt contacts (2.904(1) Å) are somewhat closer to the single bond radius sum (2.75 Å), indicating an increased covalency between Zr and Pt atoms. In addition, the average Zr–Ni distance in Zr_4Ni_2O is 2.835 Å [4] which is only slightly smaller than the average Zr–Pt distance here (2.904(1) Å), in some contrast with a ~0.15 Å difference in the single bond radii of Ni and Pt. This might indicate a stronger interaction between Zr–Pt, perhaps because of the higher Mulliken electronegativity of Pt compared with Ni (5.6 versus 4.4). Although a small deviation from the full Pt stoichiometry was refined (1.95), the deviation is only about 5σ, whereas the synthetic results indicate smaller contents can be achieved. All atomic positions were assumed to be fully occupied in Zr_4Ni_2O, the only other single crystal analysis of these ternary systems. Crystal structures of the filled-Ti_2Ni structures indicate that whereas the 48*f* and 32*e* sites are exclusively occupied by the early and late transition element, respectively, either can occupy the 16*d* site. Accordingly, the 32*e* Pt site was refined here as partially occupied rather than mixed with Zr.

A bonding analysis of the cubic oxide by means of TB-LMTO-ASA calculations (Supplementary material) reveals, not surprisingly, a metallic character for the compound, with major contribution from delocalized Zr 4*d* states. The Pt 5*d* states are relatively more localized but contributions extend up to the conduction band. Significant mixing between Zr 4*d* and Pt 5*d* states and between O 2*p* and Zr1 5*s* and 4*d* states is observed.

Earlier electronic structure calculations on Zr_4Ni_2O also revealed the presence of empty bonding states, suggesting the

possibility of additional electron doping. Following this, synthesis of several electron- richer examples, e.g., Zr_4Cu_2O and Nb_4Ni_2O, were achieved [4].

4. Conclusions

Some characteristics of the Zr–Pt–O system have been defined around the filled-cubic Ti_2Ni-type ternary oxide as well as the structure of this phase by means of single crystal diffraction. The refined composition was found to be nearly stoichiometric, $Zr_{4.0}Pt_{1.95(1)}O_{0.93(6)}$, in contrast to its mixed phase source ($Zr_4Pt_2O_{0.66}$) which also contained hexagonal $Zr_5Pt_3O_x$ in which x is probably much smaller. The latter product distinctly limits the yield of the cubic phase near its upper Pt limit.

Supplementary material

Additional files with structural data and a plot of LMTO DOS results for Zr_4Pt_2O.

CIF files for the refined structures can be obtained from the Fachinformationszentrum Karlsruhe, 76344 Eggenstein-Leopoldshafen, Germany (e-mail: crysdata@fiz.karlsruhe.de) on quoting the Registry nos. CSD–391475 (Zr_4Pt_2O) or CSD–391476 (Zr_5Pt_3).

Acknowledgments

This research was supported by the office of the Basic Energy Sciences, Materials Sciences Division, US Department of Energy; Ames Laboratory is operated for DOE by Iowa State University under Contract no. W-7405-Eng-82.

Appendix A. Supplementary material

Supplementary data associated with this article can be found in the online version at doi:10.1016/j.jssc.2009.04.011.

References

[1] F. Laves, H. Wallbaum, J. Naturwiss. 27 (1939) 674.
[2] P. Duwez, J.L. Taylor, Trans. Am. Inst. Min. (Metall.) Eng. 188 (1950) 1173.
[3] G.A. Yurko, J.W. Barton, J.G. Parr, Acta Cryst. 12 (1959) 909.
[4] R. Mackay, G.J. Miller, H.F. Franzen, J. Alloys Compd. 204 (1994) 109.
[5] M.V. Nevitt, L.H. Schwartz, AIME Trans. 212 (1958) 700.
[6] M.V. Nevitt, J.W. Downey, R.A. Morris, AIME Trans. 218 (1960) 1019.
[7] M.V. Nevitt, AIME Trans. 218 (1960) 327.
[8] W. Rostoker, AIME Trans. 203 (1955) 113.
[9] D.J. Sordelet, X. Yang, E.A. Rozhkova, M.F. Besser, M.J. Kramer, Intermetallics 12 (2004) 1211.
[10] International Centre for Diffraction Data, 12 Campus Boulevard, Newtown Square, PA 19073-3273, USA 〈info@icdd.com〉.
[11] STOE WinXPOW version 1.07, 2000.
[12] SMART; Bruker AXS, Inc.; Madison, WI, 1996.
[13] R.H. Blessing, Acta Crystallogr. A 51 (1995) 33.
[14] SHELXTL; Bruker AXS, Inc.; Madison, WI, 2000.
[15] L.M. Gelato, E.J. Parthe′, J. Appl. Cryst. 20 (1987) 139.
[16] O.K. Andersen, Phys. Rev. B 12 (1975) 3060.
[17] O.K. Andersen, O. Jepsen, Phys. Rev. Lett. 53 (1984) 2571.
[18] O.K. Andersen, O. Jepsen, D. Glötzel, in: F. Bassani, F. Fumi, M.P. Tosi, W.R.L. Lambrecht (Eds.), Highlights of Condensed-matter Theory, North-Holland, New York, 1985.
[19] O.K. Andersen, Phys. Rev. B 34 (1986) 2439.
[20] R. Tank, O. Jepsen, H. Burckhardt, O.K. Andersen, Program TB-LMTO 47, Max Plank Institut für Festkörperforschung, Stuttgart, Germany, 1994.
[21] U. von Barth, L Hedin, J. Phys. C 5 (1972) 1629.
[22] D.D. Koelling, B.N. Harmon, J. Phys. C 10 (1977) 3107.
[23] O. Jepsen, O.K. Andersen, Z. Phys. B 97 (1995) 645.
[24] R. Dronskowski, P. Blöchl, J. Phys. Chem. 97 (1993) 8617.
[25] P.E. Blöchl, O. Jepsen, O. K Andersen, Phys. Rev. B 49 (1994) 6223.
[26] J.D. Corbett, E. Garcia, A.M. Guloy, W.-M. Hurng, Y.-Uk. Kwon, A.E. Leon-Escamilla, Chem. Mater. 10 (1998) 2824.
[27] P.R. Alonso, D.E. Arias, L.M. Gribaudo, Scr. Mater. 44 (2001) 429.
[28] T.K. Biswas, K. Schubert, Z. Metallk. 58 (1967) 558.
[29] L. Pauling, The Nature of the Chemical Bond, third ed., Cornell University Press, Ithaca, NY, 1960, pp. 403.